A CAE Approach in Application of Nafion-Pt Composite (ICPF) Actuators — Analysis for Surface Wipers of NASA MUSES-CN Nanorovers —

Satoshi Tadokoro[a], Masahiko Fukuhara[a], Yoseph Bar-Cohen[b], Keisuke Oguro[c], Toshi Takamori[a]

[a]Department of Computer and Systems Engineering, Kobe University
1-1 Rokkodai, Nada, Kobe 657-8501, Japan
[b]Jet Propulsion Laboratory
4800 Oak Grove Drive, Pasadena, CA 91109-8099, USA
[c]Osaka National Research Institute, AIST, MITI
1-8-31 Midorigaoka, Ikeda, Osaka 563-8577, Japan

ABSTRACT

Nafion-Pt composite (ICPF) is one of the most practical electroactive polymer nearest to applications. In this paper, motion of ICPF was analyzed to design a dust wiper of a visual/IR window of Nanorover of NASA MUSES-CN mission by applying Kanno-Tadokoro simulation model. This is a gray-box model between input (voltage) and output (displacement) consisting of 3 stages: an electrical stage, a stress generation stage and a mechanical stage. In the electrical stage, the input is voltage and the output is distributed current through the membrane. In the stress generation stage, the input is the current and the output is internal stress. The mechanical stage is approximated by an elastic body or a viscoelastic body. Many results have shown validity of this model. As a result of analysis, the following were revealed. Strain near the electrode is lager than that at the tip. The actuator shows a rolling-up shape at the edges. The larger the aspect ratio of ICPF is, the larger the displacement is, because this spoils the actuator motion. A crosspiece at the tip prevents ICPF from rolling up and the efficiency is improved. Too long crosspiece disables ICPF from moving with a good performance.

Keywords: Electroactive Polymer, ICPF, Gray-Box Model, MUSES-CN, Wiper Design

1. INTRODUCTION

MUSES-C, which is the world's first mission that samples of an asteroid are gathered and brought back to the Earth, is planned to implement in 2002. This project is carried out under a collaboration between NASA and the Japan's Institute of Space and Astronautical Science. A miniature rover, which have been researched by JPL (Jet Propulsion Laboratory), will be used for exploration of the planetary surface and gather photos of the surface. One of the technological task of this rover is to miniaturize saving the mass under 100 grams. This project in MUSES-C mission is called MUSES-CN.

A wiper to remove dust from the visual/IR window of the rover has been researched at JPL. This dust wiper should be small and light. Large displacement to remove dust, quick response and durability are required. Nafion-Pt composite (ICPF) is one of the materials which satisfies these requirements. Advantages of the ICPF actuator are low driving voltage, quick response, high durability and possibility of miniaturization. Applications of this actuator have been studied in robotics.[1–4]

Some motion models of the ICPF actuator have been proposed. Guo et al.[1] built a model from frequency characteristics. Kanno et al.[5–7] built a gray-box model (Kanno-Tadokoro model). Shahinpoor[8,9] proposed a model consisting of 4 forces produced by ionic motion. Firoozbakhsh et al.[10] modeled ionic interactions. Shahinpoor[11] considered electrostatic force caused by the surface micro structure.

Send correspondence to S.Tadokoro
S.Tadokoro: E-mail: tadokoro@octopus.cs.kobe-u.ac.jp, Tel.: +81-78-803-6229, Fax.: +81-78-803-6390

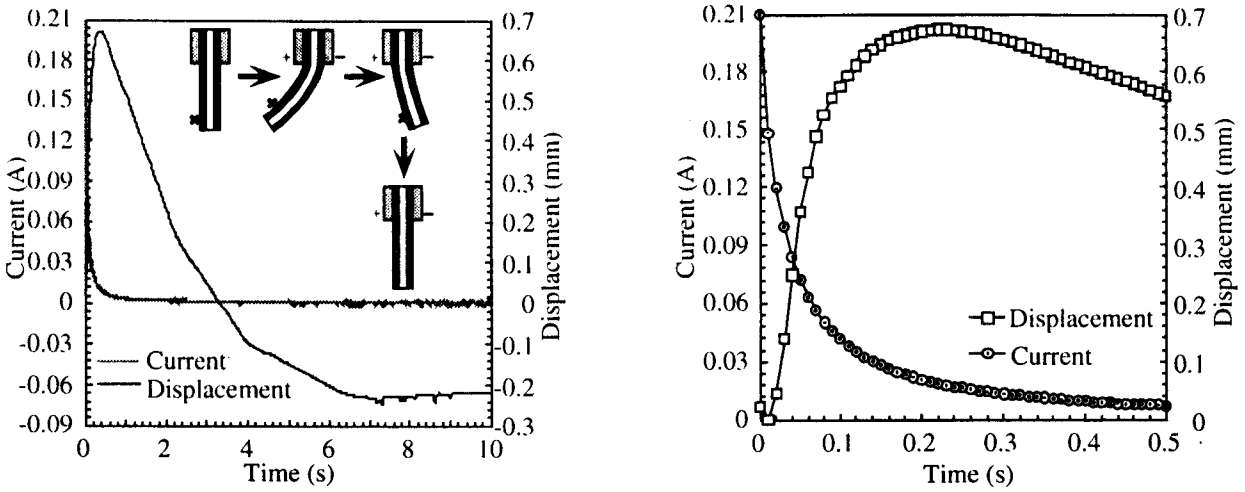

Figure 1. Response under step voltage (1.5 V).

Kanno-Tadokoro model was constructed by experimenting and analyzing the characteristics of the ICPF actuator, because the principle of actuator motion was not completely known yet. This is a gray-box model, and a part is based on physical analyses. It is composed of three stages: an electrical stage, a stress generation stage and a mechanical stage.

Computer simulation of ICPF motion to design the dust wiper was carried out by applying Kanno-Tadokoro model. The size of the ICPF actuator, a fixture at the base of the actuator and a blade attached at the tip of the actuator were considered to be elements influencing motion of the dust wiper.

In this paper, Kanno-Tadokoro model is explained, and the simulations and analyses for motion of the ICPF actuator to design the dust wiper by applying this model are described.

2. KANNO-TADOKORO MODEL

2.1. Division into Three Stages

Figure 1 shows an experimental displacement and a current curve by step voltage 1.5 V. Figure 2 shows the relations of the maximum displacement and the maximum current to the step input voltage. The experimental results show the following.

- The current through the actuator rapidly increased as soon as the voltage was applied, and decreased exponentially. The current continued to flow as a very small current while the input voltage was applied (Fig. 1).
- The actuator immediately bent toward the anode side and reached the maximum displacement after the voltage was applied. Then it bent back toward the cathode side and reached the maximum displacement on the cathode side. It continued to return to the initial position (Fig. 1).
- Both the maximum displacement and the maximum current under step voltage were proportional to the input voltage (Fig. 2).

From the above experimental results, the following principle was assumed. When voltage is applied to the actuator, current flows inside the actuator. The current is transformed into internal stress for bending motion. The relation between the input and the output is shown in Fig. 3. There are three stages in this model: an electrical stage, a stress generation stage and a mechanical stage.

Actual ICPF actuator showed nonlinear dynamic characteristics. However, it was assumed that the characteristics were linear in building the model, because the principle of actuator motion was not completely known yet.

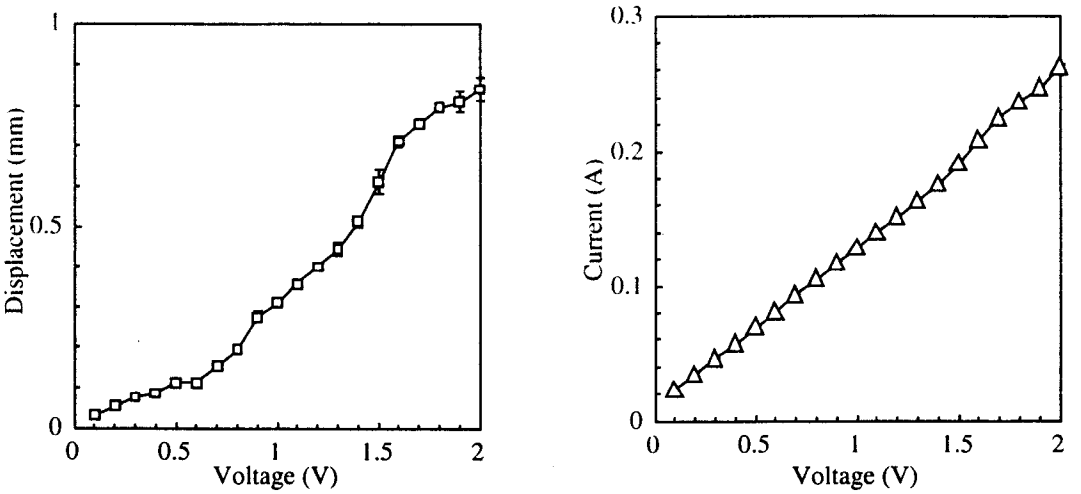

(a) Maximum displacement. (b) Maximum current.

Figure 2. Maximum displacement and Maximum current under step voltage.

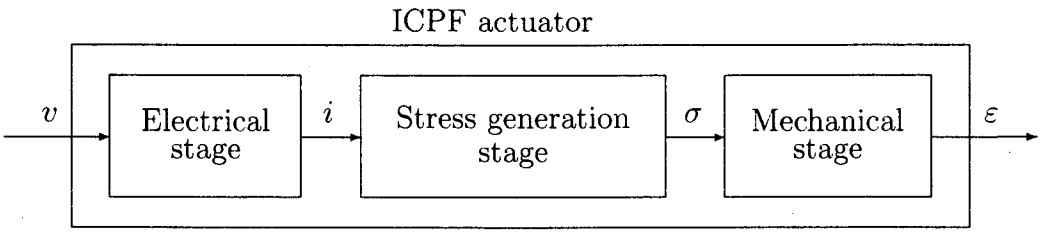

Figure 3. Three stages of Kanno-Tadokoro model (v: voltage, i: current, σ: internal stress, ε: strain).

2.2. Electrical Stage

In this stage, the input is voltage and the output is distributed current. In constructing the electrical model, the following three points were considered from the relation between the input voltage and the current (Fig. 1).

- The current rapidly increases as soon as the voltage is applied.
- The current decreases exponentially.
- The very small current continues to flow while the voltage is applied.

The electrical stage is shown in Fig. 4. The moving part of the actuator was divided into elements, where R_a (Ω) and R_b (Ω) are the resistances of the platinum layers, and R_x (Ω) is an approximate resistance of the gel permeated with water. The characteristic of the exponential decrease can be approximated to a time lag of the first order. This characteristic is approximated by a series connection of R_c (Ω) and a capacitance C (F). The transfer function of this stage is the following.

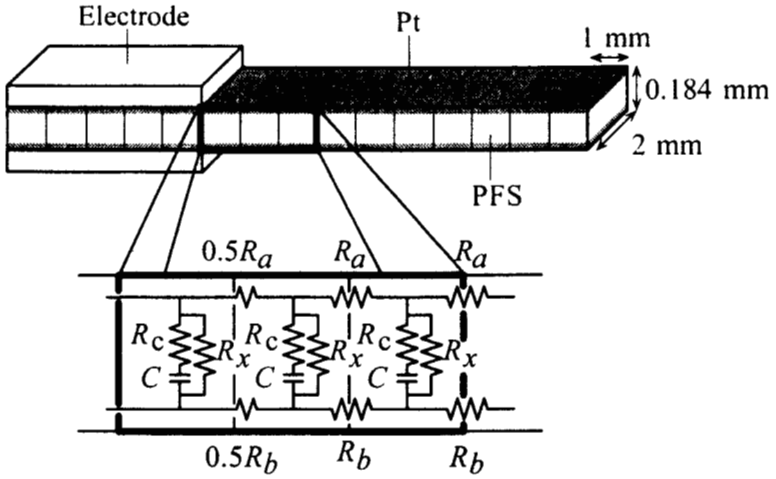

Figure 4. Electrical model.

$$G(s) = \sum_{k=1}^{n} \frac{CR_{num}s + 1}{CR_{den1,k}s + R_{den2,k}} + \alpha n \frac{CR_{num}s + 1}{CR_x R_c s + R_x} \tag{1}$$

where

$$R_{num} = R_x + R_c \tag{2}$$

$$R_{den1,k} = R_x R_c + (R_x + R_c) R_{sf,k} \tag{3}$$

$$R_{den2,k} = R_x + R_{sf,k} \tag{4}$$

$$R_{sf,k} = (k - \frac{1}{2})(R_a + R_b) \tag{5}$$

n is the elemental number of the moving part. α is the ratio of the length of the electrode to that of the moving part.

The values of the resistances R_a and R_b were calculated by using measured surface resistivities. The resistances of the gel membrane permeated with water R_x was calculated from the measured current in steady state of the step response. C and R_c were identified by comparing the simulation curve with the experimental curve of step voltage, because these values could not be measured physically. The parameters of the electrical stage are shown in Table 1.

Table 1. Parameters of the electrical model.

Parameter	Value
R_a	5.4 Ω (Resistivity: 2.2×10^{-2} Ω mm)
R_b	5.0 Ω (Resistivity: 2.0×10^{-2} Ω mm)
R_x	3.8×10^3 Ω
R_c	9.5×10 Ω
C	$2.9 \times 10^{-4} F$

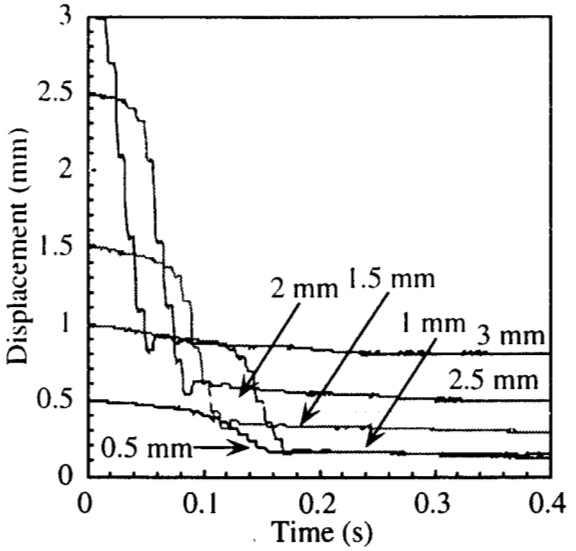

Figure 5. Free vibrations after opening fixed point of 0.5 mm from the tip.

2.3. Stress Generation Stage

In this stage, the distributed current is transformed into distributed internal stress.

The principle of the generation of the internal stress was evolved from experimental free vibration of the actuator (Fig. 5). This damping curve was obtained by releasing the tip of the actuator after giving a certain initial displacement to the tip.

At first, a response similar to that of an elastic body appeared and was damped immediately. Then a nonlinear response, which was different from the first part, appeared. From the first response, it was clear that mechanical damping was fairly large. Therefore, it was considered that the ICPF actuator did not bend back toward the cathode side by the characteristics of an elastic body of the membrane but by the generation of the internal stress for bending toward the cathode side.

If the internal stress is generated in proportion to the current through the actuator simply, the internal stress to bend back does not generate (Fig. 1, left). This is paradoxical to the above idea. Therefore, it was assumed that the internal stress was proportional to the time derivative of the current. This assumption made it possible to generate the internal stress to bend immediately toward the anode side as soon as the current rose and the internal stress to bend back toward the cathode side.

In Fig. 1, the response of the displacement from 0 s to 0.2 s was assumed to be the second-order delay. It was considered that the principle of motion of the gel membrane permeated with water was related to movement of water

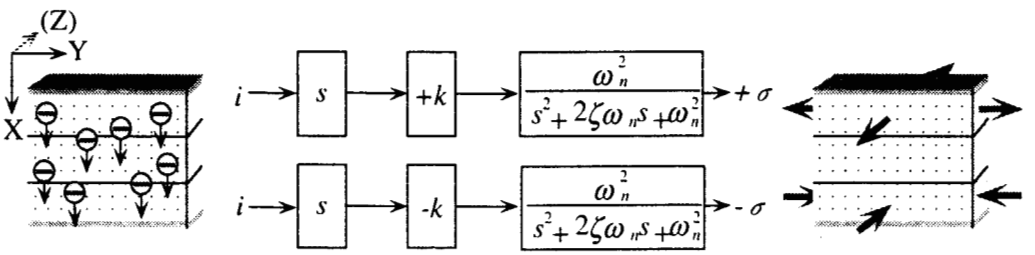

Figure 6. Signal transformation from current to internal stress for bending (Stress generation function).

in the gel.

It was assumed that the internal stress was generated at the interface between the membrane and the platinum layers.

The stress generation stage is shown in Fig. 6. The internal stress for the bending motion is in proportion to the time derivative of the current with the second-order delay. K is a stress generation tensor. The elements of the tensor are proportional factors to convert the time derivative of the current into the internal stress for bending.

In Fig. 6, when electrical charge moves in the x direction, a layer swells on one side and contracts on the other side. The signs of two proportional factors are different. This means that the each internal stress are generated in adverse directions at the two layers. In other words, the internal stress for swell is generated on one side and that for contraction is generated on the other side.

The above relation can be represented by the following expression, which is similar to that of the piezo electric elements.

$$\sigma = D(s)\varepsilon - K\{\frac{\omega_n^2 s}{s^2 + 2\zeta\omega_n s + \omega_n^2}\}I \tag{6}$$

where σ (N/m^2) is an internal stress vector, $D(s)$ is a mechanical characteristics including mass and damping, ε is a strain vector. K is a transformation tensor of stress generation. I is a current vector through the actuator. ζ and ω_n are parameters of the second-order delay.

2.4. Mechanical Stage

In this stage, the input is the internal stress and the output is displacement. The material was assumed to be an elastic body with Rayleigh damping.

The Young's modulus and damping coefficients were acquired experimentally. K, ω and ζ were identified by comparing the simulation curve with the experimental curve. Table 2 shows parameters of this model.

Table 2. Parameters of the model.

Parameter	Value
Actuator size	$10.0 \times 2.0 \times 0.184$ mm
Density	2.7×10^3 kg/m^3
Young's modulus	2.2×10^8 N/m^2
Poisson's ratio	0.3
Rayleigh damping coefficients	$\alpha = 0.5$ s^{-1}, $\beta = 0.1$ s
Stress generation coefficients	$k_{xyy} = k_{xzz} = \pm$ 176.0 Ns/m^{2}A
Coefficients of delay of 2nd degree	$\zeta = 0.6, \omega_n = 1.2$ rad/s

3. VERIFICATION OF KANNO-TADOKORO MODEL

3.1. Verification of Time Constant

Figure 7 shows a time constant at each element of electrical model by simulation and experimental time constants on both the anode and the cathode side motion under step voltage. T_{d+} is a time constant on the anode side, when the final value is the maximum displacement on the anode side. T_{d-} is a time constant on the cathode side, when the initial position is the maximum displacement on the anode side and the final value is the maximum displacement on the cathode side.

The time constant T_k of the k th element from the electrode is expressed as follows in the electrical stage.

$$T_k = C\{R_c + \frac{R_x(k-1/2)(R_a+R_b)}{R_x + (k-1/2)(R_a+R_b)}\} \tag{7}$$

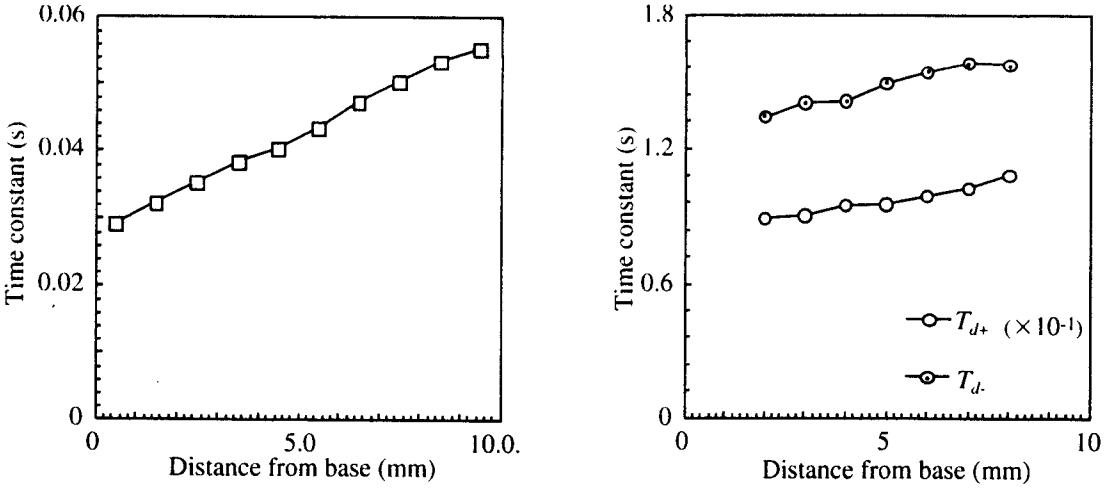

(a) Electrical stage. (b) Experiment.

Figure 7. Time constant at each element.

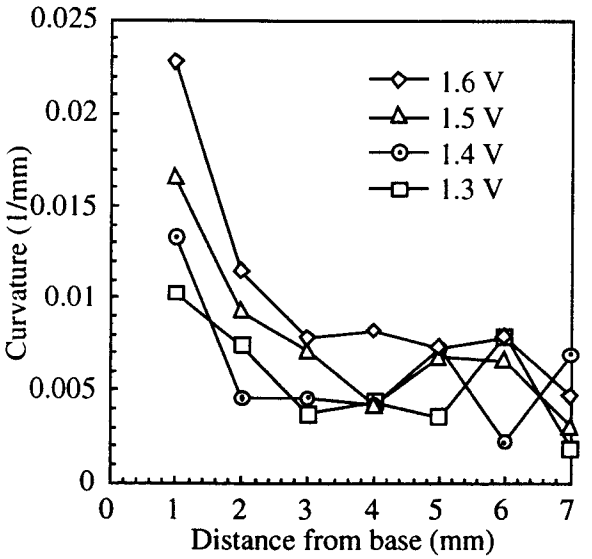

Figure 8. Experimental curvature of actuator shapes at the maximum bending under step voltage.

This shows that the time constant of each element depends on the total of resistances R_a and R_b from the electrode to the each element. The time constant near the electrode is smaller than that of the tip. Figure 7(a) shows this.

The experimental time constant near the base was also smaller than that of the tip (Fig. 7(b)).

According to this comparison, it is proved that the time constant of the electrical stage qualitatively agrees with that of the experiment.

3.2. Verification of Curvature

Figure 8 shows experimental curvatures of the maximum bending. The curvature near the base was larger than that of the tip.

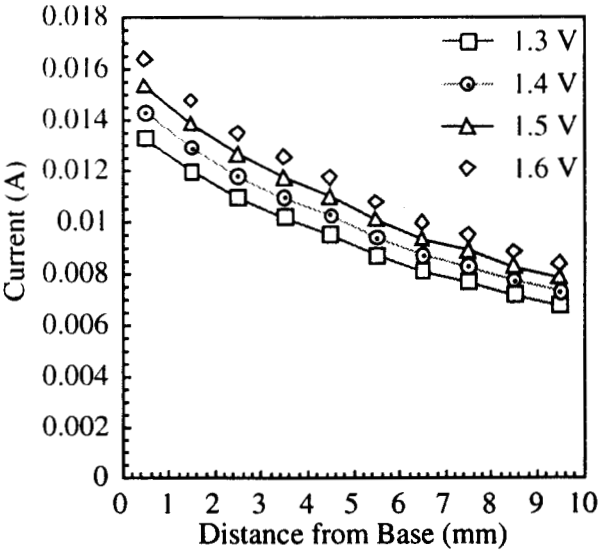

Figure 9. Simulation result of the maximum current through each element under step voltage.

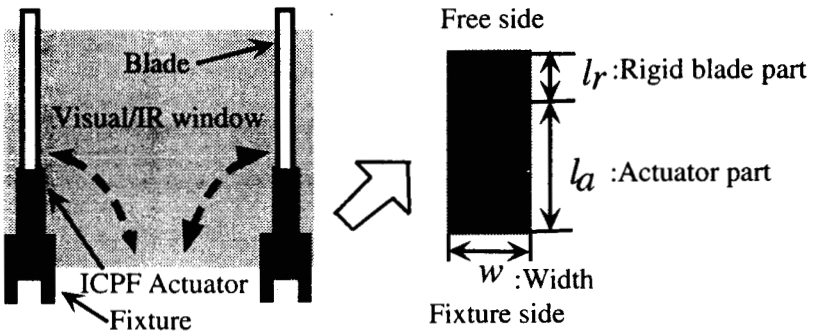

Figure 10. Schematic view of the dust wiper and simulation parameters

Figure 9 shows the maximum current of the electrical stage at each element. The maximum current near the base is larger than that of the tip. If it is assumed that current is transformed into internal stress to bend, the curvature near the base is larger than that of the tip. This qualitatively agrees with the experimental result.

According to these comparisons, it is proved that the assumption that current is transformed into internal stress can explain actual bending motion.

4. WIPER DESIGN

In this section, motion of the ICPF actuator is simulated and analyzed by using Kanno-Tadokoro model to design the dust wiper.

4.1. Method of Simulation of Dust Wiper Motion

Figure 10 shows a schematic view of the dust wiper and simulation parameters. Elements of the dust wiper are an ICPF actuator, a blade and a fixture. The blade attached at the tip of the actuator removes dust form the visual/IR window. A bias voltage (> 1 KV) will be used to repeal dust.

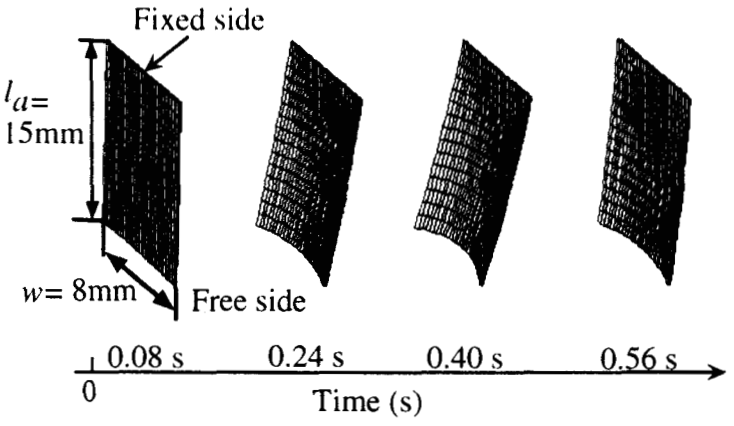

Figure 11. Simulation bending shapes of the actuator without the rigid part at the tip.

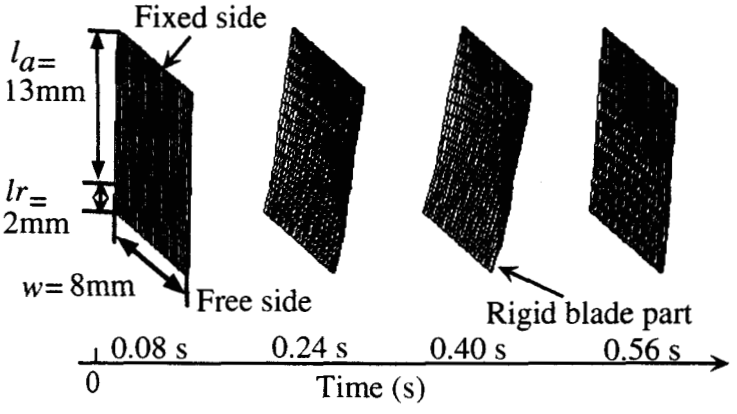

Figure 12. Simulation bending shapes of the actuator with the rigid part at the tip.

The displacement of the ICPF actuator is related to the size of the actuator. The blade prevents the tip of the actuator from bending. Therefore, the length and the width of the actuator part, and the length of the rigid part modeling the blade are considered to be parameters in the simulation. The actuator is modeled by a cantilever. Input voltage is sinusoidal waves and the output is the displacement of the actuator.

4.2. Results of Simulations

4.2.1. Comparison of bending shapes

Figure 11 and 12 show the bending shapes of the ICPF actuator without and with the rigid part at the tip, respectively.

In Fig. 11, the tip of the actuator rolls up in the direction perpendicular to the bending direction as the actuator approaches to the maximum displacement. On the other hand, the rigid part prevents the rolling-up in Fig. 12. Because of this effect, the constraint by the rigid improves the displacement characteristic.

4.2.2. Relation between parameters and displacement

Figure 13 shows an example of simulation results expressing a relation of the width of the actuator (w) and the length ratio of the rigid part ($l_r/(l_r + l_a) \times 100$) to the displacement.

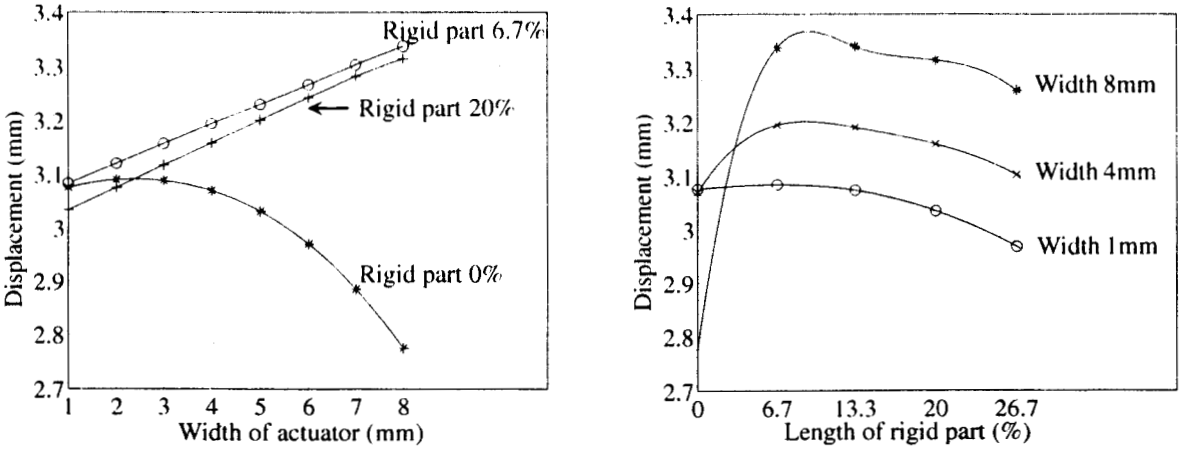

Figure 13. Relation between the parameters and the displacement.

- In regard to an actuator without the rigid part (rigid part 0 %), smaller aspect ratio of the ICPF actuator produces smaller displacement. This is because of the rolling-up shape effect. In the case of an actuator with the rigid part, the rigid part at the tip works as a crosspiece and prevents the tip from rolling up. Therefore the displacement does not become small even if the aspect ratio is small.
- Too long rigid part disables the actuator from moving with a good performance, because the length of the actuator part is short.

4.3. Analysis of Simulation Results

The following points of design were elucidated by analysis of simulation results.

- It is necessary to consider the rolling-up shape effect, because it spoils motion of the ICPF actuator. The aspect ratio of the actuator should be optimized, because the rolling-up shape effect depends on the ratio.
- Crosspieces for constraining the perpendicular actuator motion are effective to prevent the actuator from rolling up. Optimization of the size of crosspieces is important because it affects the length of actuator and its performance.

5. CONCLUSION

In this paper, the following is described.

- Kanno-Tadokoro model was applied to a dust wiper design for MUSES-CN Nanorover.
- In this model, input voltage is converted to distributed current which generates distributed internal stress. The stress generation characteristic is expressed by an equation similar to the piezoelectric equation with the second-order delay. The verifications of time constant and curvature distribution show the validity of this model.
- The ICPF actuator shows rolling-up shape at the edge in the direction perpendicular to the bending direction as it approaches to the maximum displacement. The rolling-up shape spoils motion of the actuator, and its effect depends on the aspect ratio of the actuator.
- Crosspieces at the tip of the actuator prevent the actuator from rolling up. The size should be optimized in order not to spoil the total performance.

REFERENCES

1. S. Guo, T. Fukuda, K. Kosuge, F. Arai, K. Oguro and M. Negoro, "Micro catheter system with active guide wire", *Proc. 1995 IEEE International Conference on Robotics and Automation*, pp. 79–84, 1995
2. S. Tadokoro, T. Murakami, S. Fuji, R. Kanno, M. Hattori and T. Takamori, "An Elliptic Friction Drive Element Using an ICPF (Ionic Conducting Polymer gel Film) Actuator", *Proc. 1996 IEEE International Conference on Robotics and Automation*, , pp. 205–212, 1996.
3. S. Tadokoro et al., "Development of a distributed actuation device consisting of soft gel actuator elements", *Proc. IEEE International Conference on Robotics and Automation*, pp. 2155-2160, 1998
4. S. Tadokoro, S. Yamagami et al., "Multi-DOF device for soft micromanipulation consisting of soft gel actuator elements", *Proc. 1999 IEEE International Conference on Robotics and Automation*, pp. 2177–2182, 1999.
5. R. Kanno, S. Tadokoro, T. Takamori, M. Costaftis, M. Hattori and K. Oguro, "Dynamic Model of ICPF Actuator" *Proc. 1995 IEEE International Conference on Systems, Man and Cybernetics*, pp. 177–182, 1995
6. R. Kanno, S. Tadokoro, T. Takamori, M. Hattori and K. Oguro, "Modeling of ICPF Actuator -Modeling of Electrical Characteristics-", *Proc. 1995 IEEE 21st International Conference on Industrial Electronics, Control and Instrumentation*, pp. 913–918, 1995
7. R. Kanno, S. Tadokoro, T. Takamori and K. Oguro, "3-Dimensional Dynamic Model of ICPF Actuator", *Proc. 1996 IEEE International Conference on Systems, Man and Cybernetics*, 1996
8. M. Shahinpoor, "Active polyelectrolyte gels as electrically controllable artificial muscles and intelligent network structures", Structronic Systems: Smart Structures, Devices and Systems, Part II: Systems and Control, World Scientific, pp. 31–85, 1998
9. M. Shahinpoor, Y. Bar-Cohen, J.O. Simpson, J. Smith, "Ionic Polymer-Metal Composites (IPMC) as Biomimetic Sensors", Actuators and Artificial Muscles - A Review, Field Responsive Polymers, American Chemical Society, 1999
10. K. Firoozbakhsh, M. Shahinpoor, M. Shavandi, "Mathematical Modeling of Ionic-Interactions and Deformation in Ionic Polymer-Metal Composite Artificial Muscles", *Proc. SPIE Smart Structure and Material Conference*, 1998
11. M. Shahinpoor, "Electro-Mechanics of Iono-Elastic Beams as Electrically-Controllable Artificial Muscles", Acta Mechanica, 1999